ACS APPLIED MATERIALS & INTERFACES

Article

Natural Carbonized Sugar as a Low-temperature Ammonia Sensor Material: Experimental, Theoretical and Computational Studies

Balaji Ghule, Shoyebmohamad F. Shaikh, Satish Ekar, Umesh Tukaram Nakate, Krishna Chaitanya Gunturu, Nanasaheb Shinde, Mu. Naushad, Kwang Ho Kim, Colm O'Dwyer, and Rajaram Mane

ACS Appl. Mater. Interfaces, **Just Accepted Manuscript** • DOI: 10.1021/acsami.7b13122 • Publication Date (Web): 20 Nov 2017

Just Accepted

ACS Publications

ACS Applied Materials & Interfaces is published by the American Chemical Society.
1155 Sixteenth Street N.W., Washington, DC 20036

Natural Carbonized Sugar as a Low-temperature Ammonia Sensor Material: Experimental, Theoretical and Computational Studies

Balaji G. Ghule[a], Shoyebmohamad Shaikh[a], Satish U. Ekar[a], Umesh Nakate[a], Krishna Chaitanya Gunturu[b], Nanasaheb M. Shinde[c], Mu. Naushad[d], Kwang Ho Kim[e], Colm O'Dwyer[f] and Rajaram S. Mane[a,e]**

[a]School of Physical Sciences, Swami Ramanand Teerth Marathwada University, Nanded-431606, M.S., India.

[b]School of Chemical Sciences, Swami Ramanand Teerth Marathwada University, Nanded-431606, M.S., India.

[c]Department of Materials Science and Engineering, Pusan National University, San 30 Jangjeon-dong, Geumjeong-gu, Busan 609-735, Republic of Korea.

[d]Department of Chemistry, College of Science, Bld-5, King Saud University, Riyadh, Saudi Arabia.

[e]National Core Research for Hybrid Materials Solution, Pusan National University, Busan, 600-735, Korea.

[f]Department of Chemistry, University College Cork, Cork, T12 YN60, Ireland.

CORRESPONDING AUTHOR: rajarammane70@gmail.com (Rajaram S. Mane, Prof.) and c.odwyer@ucc.ie (Colm O'Dwyer, Prof.)

ABSTRACT

Bearing in mind the advantages of useful, cost-effective and eco-friendly synthesis, carbonized sugar (CS) has been synthesized *via* microwave-assisted carbonization of market quality table-top sugar. The as-prepared CS has been characterized for its morphology, phase purity, type of porosity and pore-size distribution etc. The gas sensing properties of CS for various oxidizing and reducing gases are demonstrated at ambient temperature where we observe good selectivity towards liquid ammonia amongst other gases. The highest ammonia response (50%) of a CS-based sensor was noted at 80°C for 100 ppm concentration. The response and recovery times of CS sensor are 180 s and 216 s, respectively. This unveiling ammonia sensing study is explored through plausible theoretical mechanism which further is well-supported by computational modelling performed using density function theory. The effect of relative humidity on CS sensor has also been studied at ambient temperature, which demonstrated that the minimum and maximum (20%-100%) relative humidity revealed 16 % and 62 % response respectively.

KEYWORDS: Carbonized sugar; Structural analysis; Surface morphology; Ammonia sensor; Density Function Theory.

1. INTRODUCTION

The pressing need for environmental monitoring has ever been more important, due largely to the rising air pollution in the last few decades.[1-2] The detection of poisonous and hazardous gases in mixtures, in low quantities and under different environmental conditions can be achieved by increasing the sensitivity of gas sensors at ambient temperature. The developments in gas sensor technology must be economic, eco-friendly, chemically stable and environmentally robust[3-6] and furthermore, sensor materials should not add to the environmental risk. Researchers are actively engaged in developing sensor with such signatures.[7-8] The working principle of a gas sensor is based on a change in electrical conductivity due to surface reactions such as oxidation or reduction caused by an exposure to various gases. Chemical sensing also depends on the active centers, chemical properties and the defects existing on the surface layer of the sensor material.[9] Semiconducting metal oxides such as zinc oxide, bismuth oxide, tin oxide, iron oxide, titanium dioxide etc., are being studied to develop cost-effective gas sensors specific to various gases.[10-12] However, metal oxide-based gas sensors have several limitations such as expensive metal salts, toxicity, high operating temperature, chemical instability etc.[12,13] It is widely accepted that sensors based on metal oxide nanostructures have limited surface area and require elevated temperatures for their efficient operation; a pressing goal is to reduce operating temperature without any loss of gas sensitivity.

In recent years, carbon-based materials such as carbon nanotubes, graphene and graphene oxide etc., have shown excellent gas sensor properties.[14-18]The natural carbon sources, used for the synthesis of functional carbon materials, and their applications have also been studied by different groups of researchers worldwide. Yuan *et al.* presented a facile and green strategy for fabrication of carbon-foam with tunable pore structure by controlling the amount of yeast and water in bread.[19] Rybarczyk *et al.* fabricated a series of carbon materials from natural rice husk and further envisaged in Li−S battery.[20] Carbon-based materials are a potential next generation gas sensor material for autonomous sensor

technology, since they have excellent detection sensitivity with interesting energy conversion characteristics.[21] The absence of certain atoms and the reconstruction of the lattice due to annealing leads to most of the intrinsic defects in the carbon nanostructure.[22] The intrinsic defects in carbon nanostructures include point defects (vacancies, Stone–Wales defects) and line defects (dislocation, grain boundaries) and in-plane topological defects (non-hexagonal rings, such as pentagons and heptagons), which undoubtedly break the electron–hole symmetry, alter the local density of the π-electrons, increase the chemical reactivity, and modify the edges and induce expected local active sites.[23]

There are several methods reported in literature for synthesizing carbon nanostructures which are not limited to synthetic methods such as chemical vapor deposition, arc discharge, laser ablation, microwave-assisted synthesis, hydrothermal synthesis, and atomic layer deposition[24-30] to name a few. Among these synthesis methods, microwave-assisted synthesis has several advantages such as rapid heating, fast processing, cleanliness, inexpensive, and economical infrastructure. Microwave heating has many merits over traditional heating which provides increased reaction kinetics due to its unique operation style. Rapid initial heating provides enhanced chemical reaction rate, which results in cleaner reaction products with higher yields,[31-33] and is a productive route to nanostructuring of a range of oxides and carbons[34]. Volatile Organic Compounds (VOCs) such as liquid ammonia, benzene, acetone, ethanol, formaldehyde, benzaldehyde, methanol, toluene etc has attracted researchers, because they not only pollute the environment but also directly affect human's health. In spite of that, VOCs are still used in industries to produce other chemicals and research purpose. The exposure to such hazardous VOCs is highly probable; hence, the advancement of sensors for early detection of flammable and toxic agents is necessary. The presence of high ammonia levels in the environment has adverse effects on human health. For example, it is the by-product of livestock or industry,[35] which is non-controllable and its 0.1% occurrence can cause long-term respiratory system disorder and a concentration ~0.5−1% can be lethal. Additionally, exposure to ~50 ppm ammonia level in air causes human health hazards such as

permanent blindness; lung and skin diseases etc.[36] The detection of ammonia under ambient conditions using green technology for environmental pollution monitoring is a high priority.

In the present work, we showed microwave-assisted synthesis of carbonized sugar (CS) using market quality sugar. This scalable and cost-effective method forms a carbonaceous product that is nanocrystalline, mesoporous, and exhibits a high surface area. In addition to the effectiveness in gas sensing applications, in presence of various oxidizing and reducing gases, the structure, morphology, porosity, pore-size distribution etc., has been detailed by physical analysis. The selectivity of a CS sensor was determined for various gases where CS was more selective to ammonia (NH_3) gas allowing the transient response to be recorded to measure the overall response and recovery times. The gas sensing mechanism was proposed *via* its band structure. The NH_3 sensing was studied at different concentrations to determine repeatability and stability. Finally, the results were compared with proposed theoretical model which further was confirmed from computational models designed specifically to probe of similar gas molecules such as NH_3 and chlorine (Cl_2) with CS (considered Graphene Oxide (GO) slab as Raman scattering spectrum and XPS analysis of CS closely matched with GO).

2. EXPERIMENTAL

2.1 Synthesis of Carbonized Sugar (CS)

A typical method to synthesize CS includes periodic microwave heating of dry table sugar. Initially, dry table sugar was crushed in a mortar pestle (to form a powder) and transferred into a glass beaker. The powdered sugar was heated at 300-350 W power for 15-20 mins using microwave oven. The processed powder was black in color, which was then crushed followed by air annealing at 450 °C for 2 h in an open ceramic crucible. The product yield was ~30% (~6 g) of the used synthesis material. The obtained black powder was observed to be insoluble in water, ethanol, methanol, benzene solvents at warm conditions (≤100°C) but still partially soluble in dimethyl sulfoxide (DMSO). The annealed powder was used for various characteristic measurements.

As per as synthesis of graphene oxide (GO) is concerned it was introduced quite a few decades ago by Brodie, Staudenmeier and Hummers *et al*.[37] and still continue in use today with only slight modifications. Regrettably, both Staudenmaier technique and the Brodie methods generate ClO_2 gas, which is highly toxic and has tendency to decay in air to produce explosions.[38] The Hummers method with its comparatively shorter reaction time and lack of dangerous ClO_2, is preferred by several research groups for preparing GO. One disadvantage of this method is severe contamination by excess permanganate ions, which is supposed to be removed by treatment with H_2O_2 followed by washing and thorough dialysis.[39] So we consider the microwave-assisted combustion method to synthesize the CS as a more facile, eco-friendly and cost-effective with compared to the above mentioned methods used while synthesizing commercial GO. Time consumption and an easy synthesis method are few advantages of this method over reported earlier and also commercially available GO.

2.2 Characterization details

The structure of CS was confirmed by X-ray diffraction (XRD, D8-Discovery Bruker, Cu Kα, 40 kV, 40 mA) pattern, scanned from 20 to 80°. Field-emission scanning electron microscopy (FE-SEM, Hitachi, S-4800, 15 kV) along with energy dispersive X-ray analysis (EDX) analysis and high-resolution transmission electron microscopy enclosed with SAED pattern (HR-TEM, Technai F20) were used to observe the surface morphology, grain-size and elemental configuration, respectively. X-ray photoelectron spectroscopy (XPS, VG Scientific ESCALAB250) was utilized to analyze the chemical composition and bonding status of the CS. The XPS spectrum of the CS was calibrated to the carbon peak C 1s at 284.6 eV. Raman spectrum was recorded on a WITec system within a Raman shift of 1000 cm^{-1} to 2000 cm^{-1}. The Brunauer–Emmett–Teller (BET) surface area was obtained using a Micrometrics ASAP2010 analyser in N_2 environment with proper moisture removal from the sample by heating nearly 200°C for 2 h.

2.3 Sensor Measurements

A schematic illustration of the sensor unit with a gas sensing experimental setup is shown in Figure 1. The gas sensor unit consists of a stainless-steel cylindrical chamber with 250 mL volume capacity. The

cylindrical chamber consists of heater with PID controller to set the desired temperature. A voltage stabilizer is used to provide constant voltage to avoid the fluctuations in the temperature. The change in resistance of the sensor, due to the presence of target gas, can be recorded by using Computer assisted 6-digit Keithley 6514 System electrometer. Keithley electrometer was coupled to the computer via RS232 interface to record the change in resistance with respect to time. For gas sensor studies, pellets of 1.5 cm (diameter) and 0.5 mm (thickness) area were prepared using a hydraulic pressing machine. For electrical contacts silver paste, on the sensor pellet, was preferred. The target gases used in the experiments were obtained (Cryo gases Pvt. Ltd, Mumbai, India) in 0.5 L canisters with each of 1000 ppm concentration capacity with N_2 as secondary component. The gas response was calculated from the following relation;

$$S(\%) = \frac{R_a - R_g}{R_a} \times 100 \qquad (1)$$

where, R_a is the stabilized resistance of the sensor material in presence of air, R_g is the stabilized resistance in presence of the target gas. The desired concentration of ammonia gas was obtained by the static liquid gas distribution method, which was calculated by the following formula.[40]

$$\mathrm{C\ (ppm)} = \frac{22.4\rho TV'}{273MV} \mathrm{X}\ 1000 \qquad (2)$$

where, C (ppm) is the desired target gas concentration; ρ is (g/mL) the density of the liquid; 'V' is the volume liquid ammonia (μL), T is testing temperature (K) M is the molecular weight of ammonia (g mol^{-1}), and V is the volume of testing chamber (L). In this work, the values of M, ρ, V and T are 17.03 g mol^{-1}, 0.68 g cm^{-3}, 0.250 L and 298 K, respectively.

3. RESULTS AND DISCUSSION

3.1 Surface morphology and structural elucidation

The surface morphology of the CS was revealed by performing FE-SEM (Figure 2a) and TEM (Figure 2b). It was observed from the microscopy images that CS mainly comprises globular structures. Figure S1 shows the elemental analysis of CS which clearly had shown the presence of only C and O elements. The Figure 2c and Figure 2d presents images of HR-TEM and SAED pattern where irregular grains of 10-50 nm dimensions and nanocrystalline signature are clearly evidenced. Obtained ~0.38 nm

and ~0.28 lattice spacing's are corresponding to the (002) and (100) planes, respectively, evidenced from ring diameter measured while scanning, of GO. The XRD pattern of the CS sample is shown in Figure 3a, where two broad peaks at ~26° and 43° were indexed to the (002) and (100) (#JCPDS 41-1487 for GO) planes, respectively.[41] The lattice fringe widths corresponding to (002) peak of d-spacing 0.37 nm and (100) peak of d-spacing 0.28 nm matched closely to the HR-TEM inter-planar distances. The Raman spectrum (Figure 3b) of CS demonstrated two characteristic bands at 1379 cm^{-1} (D-band) associated with sp^3 and 1592 cm^{-1} (G-band) corresponding to sp^2 graphitic configurations. The intensity ratio of the D-band over the G-band (ID/IG) was 0.75, which signifies the graphitic behavior of CS.[42] The FTIR spectrum (Figure 3c) shows broad and strong bands at ~3390 and 1090 cm^{-1} attributed to stretching vibrations and in-plane bending vibration of –OH/H_2O. A weak band at ~2926 cm^{-1} corresponds to the stretching vibrations of the C-H bond. Featured band at ~1622 cm^{-1} suggested the stretching of C=C. A relatively sharp band at ~1205 cm^{-1} confirmed stretching of –C-O or bending of alkyl groups. Band appeared at 618 cm^{-1} was assigned to C-H deformation. The assignment of all FTIR peaks was in good agreement with literature values[43] for graphitic carbon. As shown in Figure S2, the XPS survey of the as-prepared sample demonstrates the presence of C and O without any additional impurities which is in accordance with EDX analysis. The de-convoluted high resolution C 1s XPS spectrum of CS is shown in Figure 3d. The calibration of C 1s peak at a binding energy of 284.6 eV corresponds to the sp^2 carbon phase. The C 1s peaks fitted with three contributions; *sp2* (284.6 eV), C-O (286.8 eV), C=O (288.9 eV) which exactly matched with the reported values of GO,[44] so we propose that CS was similar to GO. The amount of oxygen in the CS can be explained by bonding of oxygen to defective carbon bonds. The N_2 adsorption-desorption analysis was carried out to further demonstrate the specific surface area and porous nature of the prepared CS (Figure 3e). Hysteresis loop of the adsorption-desorption curves revealed the porous nature of the CS sample. The shape of the isotherms represented a type IV hysteresis according to the IUPAC classification as the relative pressure (P/Po) was > 0.3, exhibiting a typical mesoporous (10–50 nm) signature of CS. Consequently, the specific surface area of the CS was ~5.15 m^2/g. Thus, the carbonization of sugar was an efficient method to

produce porous carbon material with a mean pore-diameter of ~4.6 nm and a pore volume of ~0.0876 cm^3/g.

3.2 Thermogravimetric analysis

Thermogravimetric analysis (TGA, Figure S3) curve presents the weight loss of CS as variation of temperature at a heating rate, 1°C/min under N_2 environment. Mass losses at two different temperatures are evidenced. The first one is minor weight loss (~ 4 wt.%) before 100 °C, probably due to evaporation of water molecules that are contained in the material.[45] While, the second one is the major one which is ~49 wt.% between 200 and 500 °C,[46] which corresponds to CO, CO_2, and steam release[10] from the most labile functional groups. Between 500 and 750 °C, CS confirms a slower mass loss which can be attributed to the elimination of more stable oxygen functionalities.[47]

3.3 Electrical properties

The electrical properties of CS sensor (pellet) were recorded as function of temperature (Figure 4). In accordance with other studies[48], the resistivity of the sensor dropped with increase of the operating temperature (Figure 4a). This drop in resistance was attributed with electron hole-pair formation. The increase in charge concentration as function of temperature was plotted and shown in Figure 4b. Due to an involvement of defective active sites, there was noticeable drop in resistance and increase in the charge concentration with temperature, demonstrating an n-type semiconductor behavior of CS sensor.

3.4 Gas sensing properties

The gas sensing properties were investigated by exposing the gas sensors to various concentrations (10 – 400 ppm) of NH_3. The gas sensing principle is based on the change in the resistance of the sensing material, which is influenced by the adsorption-desorption process of target gas molecules *via* charge transfer processes. As-discussed earlier, the CS powder was used to make a pellet and its gas sensing properties were tested. The resistance of the CS pellet was stabilized before exposure to NH_3. CS was exposed to various gases viz., NH_3, CO_2, NO_2, Cl_2 and H_2S to a maximum of 100 ppm. The CS sensor exhibited good selectivity towards NH_3 as compared to other gases (Figure 5a). We observed that the sensor resistance decreased rapidly with NH_3 exposure compared to the time taken to reach

equilibrium/saturation. The sensor testing chamber was opened to external environment through a small opening without disturbing the pressure conditions to evaluate the recovery. We also evaluated the effect of operating temperatures on sensor performance for a fixed 100 ppm NH_3 concentration in Figure 5b. It was clearly observed that the CS sensor demonstrated a maximum response of 50% to 100 ppm NH_3 at 80°C. At lower temperatures (≤80°C), adsorbed moisture water molecules could slow down the rate of adsorption of NH_3 molecules, which might limit the response. At 80°C, the desorption of water molecules takes place and the NH_3 molecules could gain energy due to the thermal excitation and try to get adsorbed at the surface of CS. The higher temperatures (≥80°C) could restrain the gas adsorption by increasing the exploitation rate of the CS sensor. Secondly, the NH_3 molecule is highly unstable at higher temperature which could result into lower response values. Therefore, the optimum temperature of CS sensor was fixed to 80°C and the same was applied in following measurements. The transient gas response time for ammonia sensing (for 90% change in resistance from its original value to its saturation) is shown in Figure 5c. The response and recovery time signatures depend on the rate of gas molecule diffusion to the surface (adsorption and desorption) and the associated reaction rate between the target gases molecules with the sensor element. The CS sensor exhibited a sensitive response of 50% to 100 ppm NH_3 gas at 80°C temperature with fast response (180 s) and recovery (216 s) times. On the exposure of NH_3 to the CS sensor, the resistance of carbon decreased from 27.5 GΩ to 13.5 GΩ in a response time of 180 s (Figure 5d). The response of CS as a function of time at various NH_3 concentrations at 80°C is shown in Figure 5e and 5f. Furthermore, the CS sensor was able to detect a lower NH_3 concentration up to 10 ppm with a response of 14%. The lower response implies less NH_3 molecules adsorption and sensing reaction at lower concentration. At high concentration, the better response was due to the greater number of NH_3 gas molecules adsorbed to react. The repeatability study of carbon sensor was performed by repetitive gas response measurements at 100 ppm NH_3 concentration and the corresponding results are illustrated in Figure 5g. The CS material helped to create a stable sensor for NH_3 as which was evidenced when CS sensor was operated for seven days at a fixed

concentration of 100 ppm NH_3 at 80°C (Figure 5h), a maximum initial response of 50% to 100 ppm NH_3 was maintained and after seven days, a slight decrease in response to 48% was found.

3.5 Gas sensing mechanism

It is known that the gas sensing mechanism of semiconducting metal oxides principally depends upon the change in electrical resistance of sensing material, which is chiefly caused by means of the adsorption/desorption of target gas molecules on the top of sensor surface, upon the interaction of different target gases. Here, we consider that the NH_3 sensing mechanism of CS sensor can be attributed to the surface adsorption phenomenon. As the CS sensor was exposed to air, oxygen molecules from air could adsorb on the CS sensor surfaces by trapping electrons form the conduction band of CS, ensuring the formation of an electron depletion layer (Figure 6) with higher resistance. Adsorbed oxygen has temperature dependent character[49] which is in O_2^- nature below 100 °C, O^- in between 100-300 °C, and O^{2-} above 300°C. When reducing NH_3 gas molecules comes in the contact with CS sensor, the formerly adsorbed oxygen species interacted with the gas molecules by setting free the trapped e^- back to the conduction band of CS sensor. In so doing, the resistivity of CS sensor decreased due to the reducing nature of NH_3 which could lead to the reduction in the width of electron depletion layer (Figure 6). The probable sensing reaction mechanism could be as follows:[50]

$$O_{2\,(air)} \longrightarrow O_{2\,(ads)} \quad (3)$$

$$O_{2\,(ads)} + e^- \longrightarrow O_{2\,(ads)}^- \quad (4)$$

$$NH_{3\,(gas)} + 5O_{2\,(ads)}^- \longrightarrow 4NO + 6H_2O + 5\,e^- \quad (5)$$

3.6 Humidity sensing activity

The humidity-sensing of the present sensor was investigated by using the two-electrode film introducing to different relative humidity (RH) conditions. RH conditions were accomplished by saturated salt solutions at room temperature (27 ˚C). Figure 7a shows the resistance of CS sensor at 20% RH conditions. From the resistance curve, we found that the resistance of the sensor decreases with the relative humidity which confirms that the H_2O molecules from the saturated salts are electron donors and results in *n*-type doping. The H_2O molecules adsorbed on the surface of sensor alters the Fermi level

nearer to the conduction band edge. Moreover, the humidity sensing mechanism is associated with the adsorption of H_2O molecules on the surface of sensor material.[51] The response time of 42 s and recovery time of 6 s are obtained for the CS-based sensor (Figure 7a). The quick recovery is attributable to the hasty desorption process of H_2O molecules from the CS surface, and the sluggish response is as a result of hydrophilic surface of the CS resulting in slow adsorption of H_2O molecules on the surface of CS sensor. The effect of different RH conditions on the sensor sensitivity is given in the Figure 7b, which confirms that the response of the sensor towards humidity increases with increase in the RH.[52-56]

3.7 Gas sensor: Computational analysis

Based on the gas sensing results, it was concluded that the carbon sensor exhibits NH_3 sensing properties at lower temperature with quite good response and recovery time values. The experimental characterization of CS in present study was well matched with the reported GO.[57, 58] Thus, we adopted a representative model of GO from the earlier reports and studied the gas phase interactions[57] to determine the basis for the selectivity of CS towards NH_3. The geometrical optimizations were carried out at M05-2X/6-31G (d) level using Gaussian09 software.[59] The analytical frequency calculations were computed at the same level and the minimum on the potential energy surface was confirmed by all positive frequencies. The binding energy evaluation was determined according to $BE = E_{(CS-G)} - (E_{CS} + E_G)$ where, $E_{(CS-G)}$, E_{CS} and E_G are the total energies of gas molecule-adsorbed CS, CS and gas molecule respectively. Among the above-mentioned gas molecules, highly selective reducing NH_3 and poorly selective oxidizing Cl_2 molecules were analyzed. The molecular electrostatic potentials (MEP) of the pure CS, CS -NH_3 and CS -Cl_2 were obtained and given in Figure 8. The charge polarization due to –O–, –OH and –COOH functional groups was clearly seen by keeping the rest of the part almost neutral. Hence, the gas molecule interactions were expected to be at these functional groups of CS. As expected, NH_3 molecule has strong hydrogen bonding interactions to both the –OH groups with 0.1783 nm and 0.2101 nm bond lengths, respectively. This results in a large binding energy of -15.0 kCal/mol.

and the associated charge polarization is clearly seen in the MEP representation. The relatively poor performing Cl_2 molecule had a minimum effect on the electronic distribution within CS. This was resembled in the MEP picture and the associated binding energy was just -10 kCal/mol. Hence, the reducing NH_3 molecules were identified *via* better interactions with CS compared to oxidizing Cl_2 molecules, which corroborates the sensitivity and response from resistance changes from charge transfer upon gas molecule binding to the CS surface. The sensor performance of the CS material was compared with reported data shown in Table 1. From this comparison, our CS sensor showed significant improvement in response and operating temperature over reported values of carbon-based sensors. Thus, the observed sensing properties of carbon derived from carbonized sugar makes it potential candidate for a low operating temperature NH_3 sensor. However, the present response of the CS sensor is not that much convincing at lower temperatures, so we are trying to improve the response as a part of future investigations either by catalytic metal like silver, gold, palladium etc., nanoparticles. Owing to the observed gas sensing results we concluded that the microwave assisted synthesized CS sensor exhibits better-quality NH_3 sensing properties at lower temperature with quite good response and recovery time values. In addition, CS sensor is able to detect a lower 10 ppm concentration of hazardous NH_3 with considerable response. Thus, the observed sensing properties of CS sensor make it appropriate candidate for the detection of hazardous NH_3 at lower temperatures.

4. CONCLUSION

In summary, CS was successfully synthesized from naturally abundant table quality sugar using an eco-friendly and cost-effective microwave-assisted synthesis method. As-synthesized CS was nanocrystalline and mesoporous with grain-sizes of 10-50 nm, and showed an excellent selectivity towards ammonia gas among the various oxidizing and reducing gases. The CS sensor displayed a high response of 50% to 100 ppm NH_3 levels at 80°C. The lowest ammonia detection level was 10 ppm with a reasonable response of 14%. In all cases, we found good repeatability and stability for CS-based

sensors. Theoretical and computational modeling studies confirmed a preferentially larger binding energy to NH_3, indicating its more favorable interaction with the carbon surface to that of other gases.

ASSOCIATED CONTENT

Supporting Information

The supporting information contains the quantitative analysis of Energy Dispersive X-ray (EDX), Binding energy survey spectrum (XPS), and Thermo-gravimetric analysis (TGA) of the CS sample. The Supporting Information is available free of charge on the ACS Publications website at DOI: 10.1021/acsami.00.

AUTHOR INFORMATION

CORRESPONDING AUTHOR:

rajarammane1970@srtmun.ac.in (R.S. Mane, Professor) and c.odwyer@ucc.ie (Colm O'Dwyer, Prof.)

ACKNOWLEDGMENTS

Authors also extend their appreciation to; a) Global Frontier Program through the Global Frontier Hybrid Interface Materials (GFHIM) of the National Research Foundation of Korea (NRF) funded by the Ministry of Science, ICT &Future Planning (2013M3A6B1078874), b) the International Scientific Partnership Program ISPP at King Saud University for funding this research work through ISPP#0032, and c) Science Foundation Ireland under grant no. 14/IA/2581. SFS would like to thank University Grants Commission, New Delhi for awarding D. S. Kothari Post-Doctoral Fellowship scheme (F.4-2/2006 (BSR)/CH/16-17/0015).

FIGURE CAPTIONS:

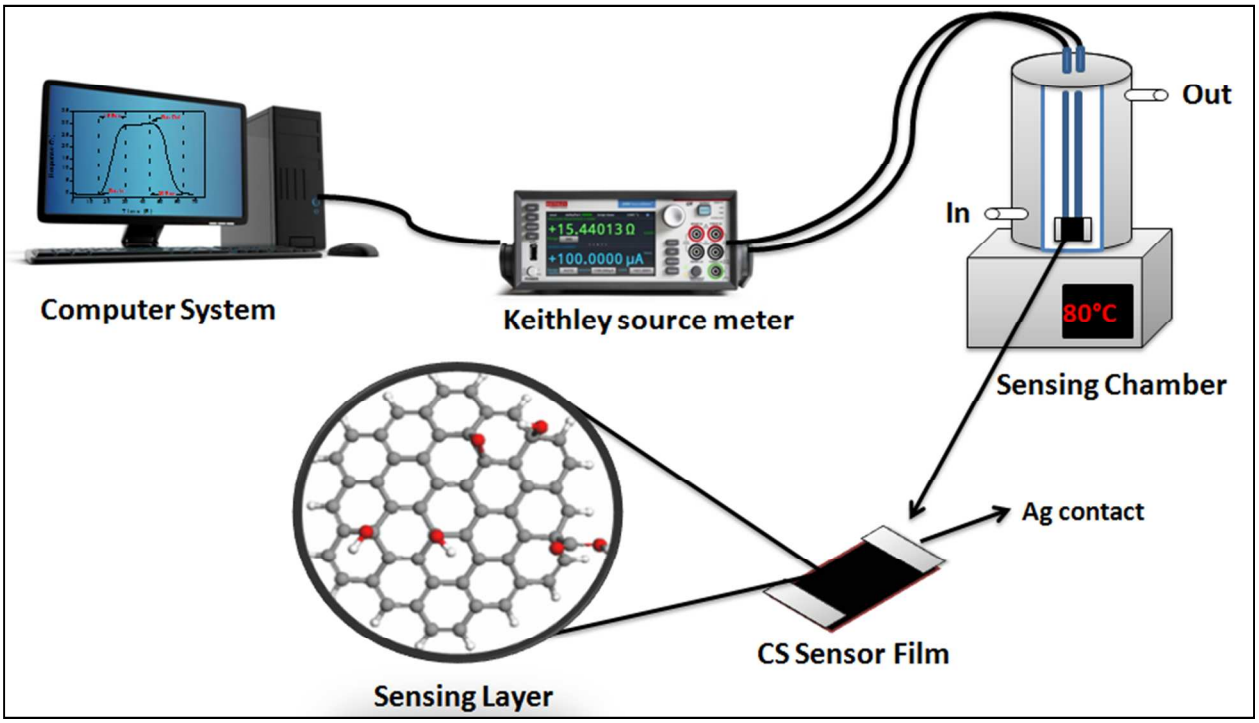

Figure 1: Schematic representation of gas sensor experimental setup.

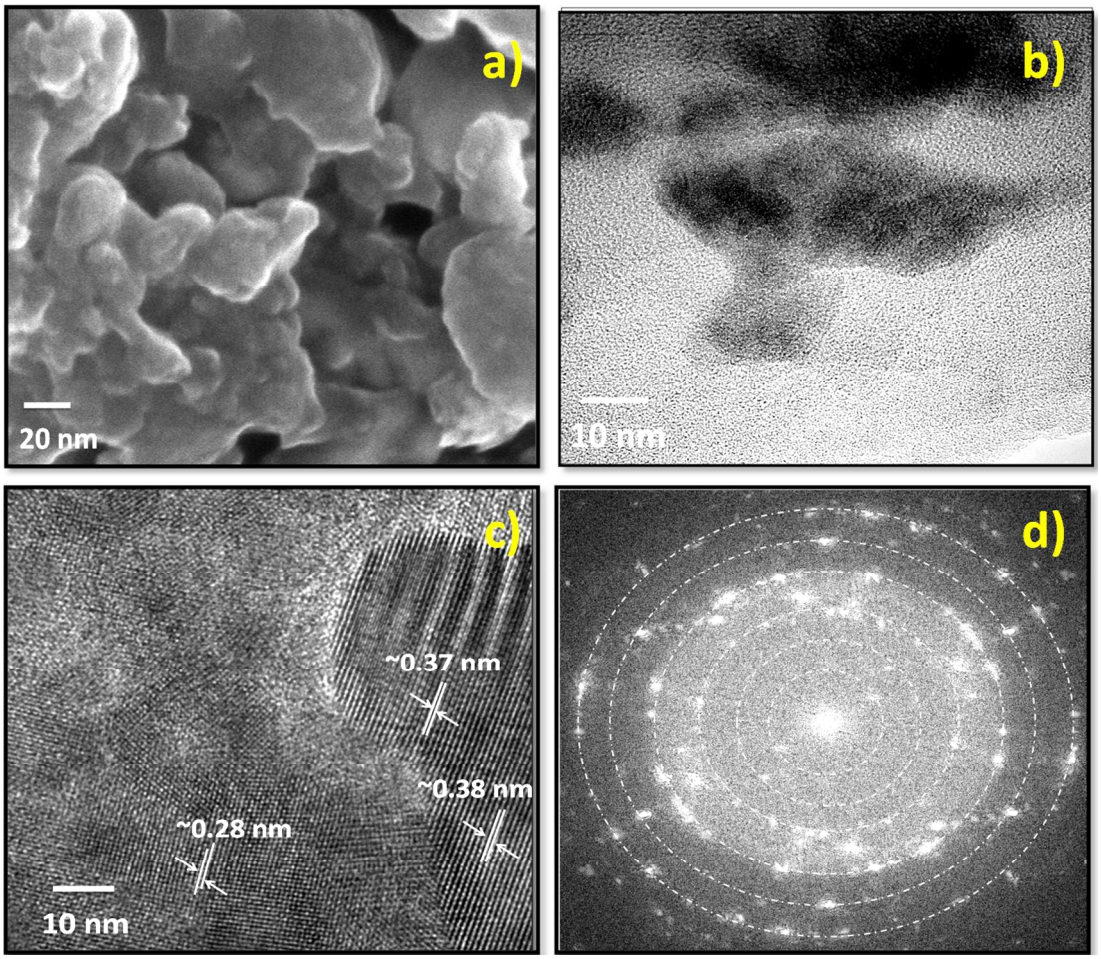

Figure 2: a) SEM shows the agglomerated nanoparticles arranged stack on top of each other. b) TEM shows the nanoparticles with smooth surface with average diameter 20-50 nm. c) HR-TEM image of CS showing clear fringes of ~ 0.38 nm and ~ 0.28 nm width. D) SAED pattern confirming the polycrystalline nature of carbonized sugar carbon.

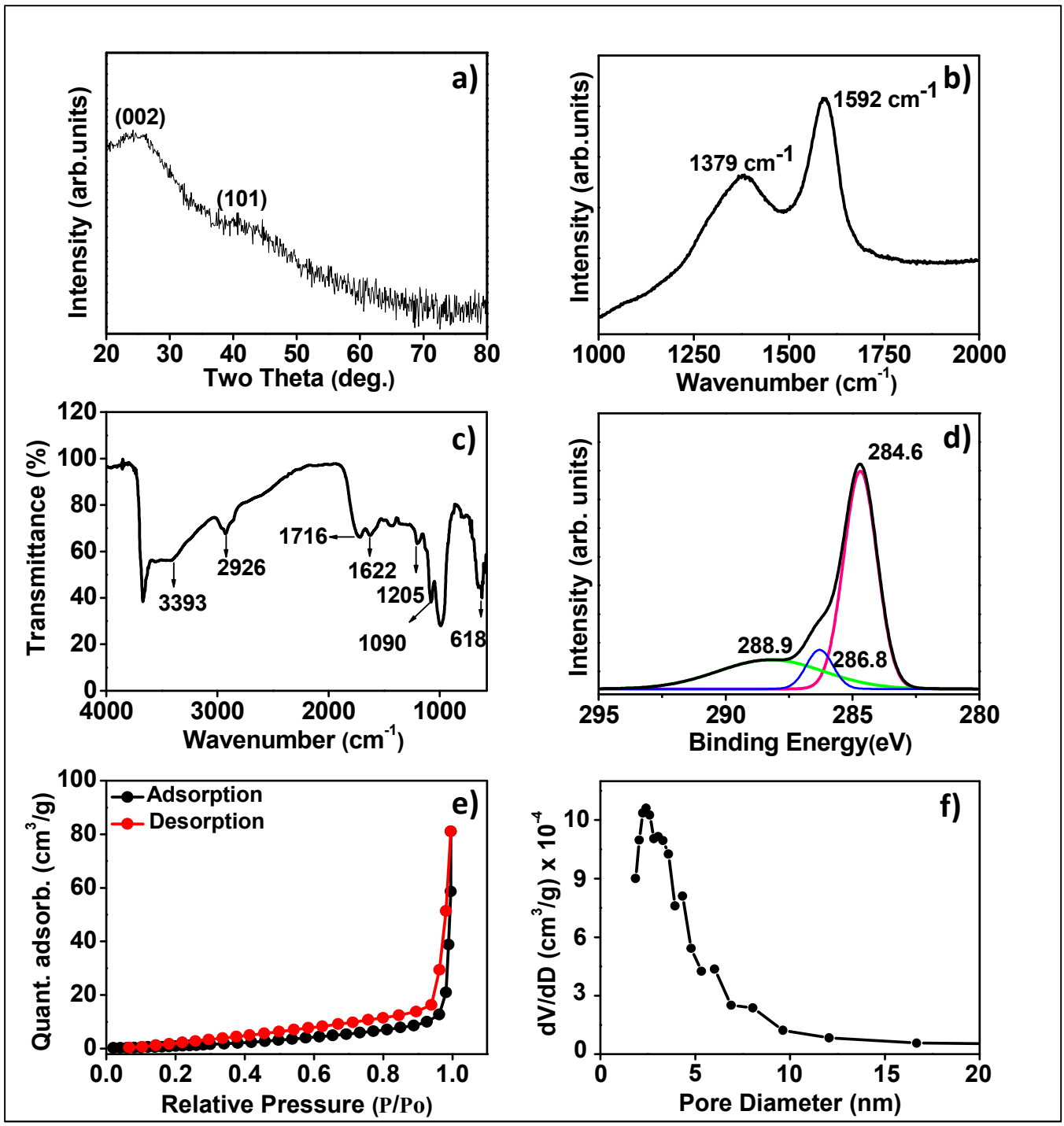

Figure 3: a) XRD pattern of CS, b) Raman shift, c) FTIR spectrum analysis, d) XPS analysis: C 1s core-level photoemission measurements of CS. e) Adsorption-desorption isotherms, and f) pore-size distribution plot for as-made CS.

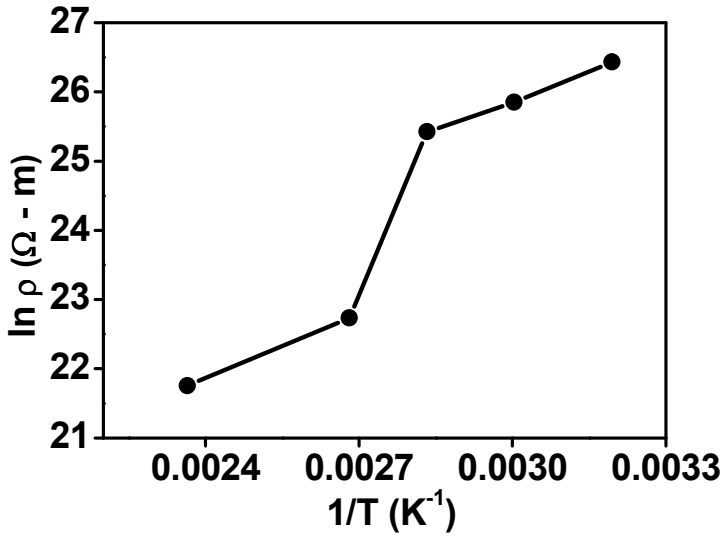

a)

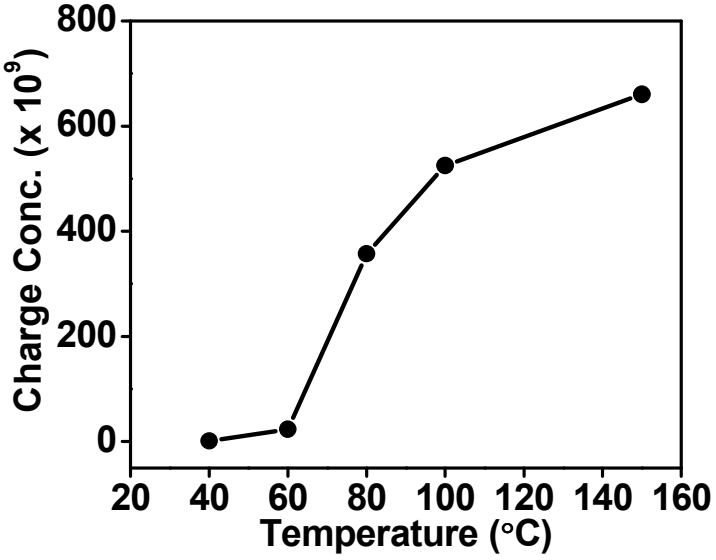

b)

Fig. 4: Electrical properties of CS sensor a) Variation of resistivity of CS with respect to temperature, b) Charge concentration in the CS sensor with respect to temperature.

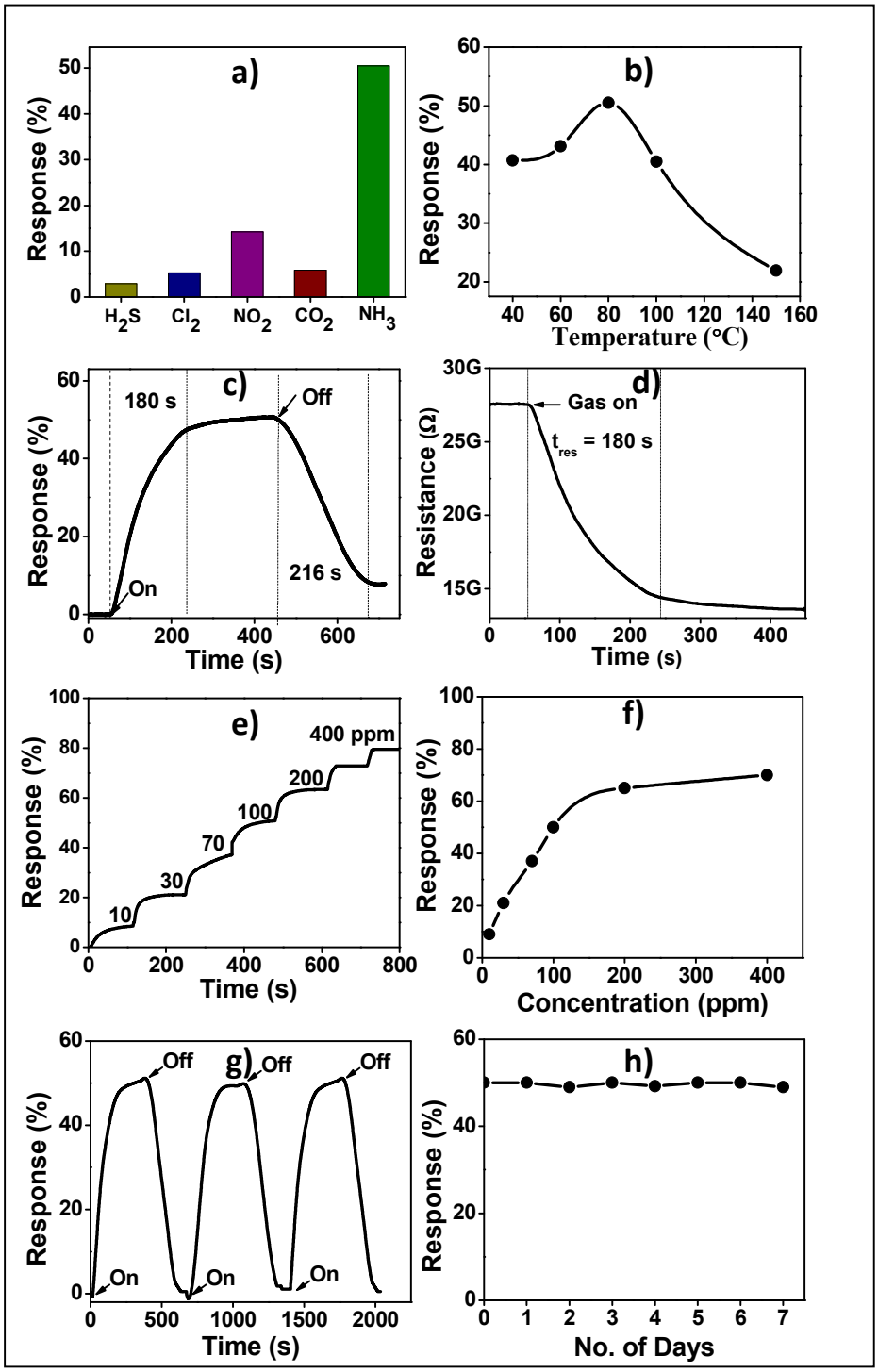

Fig. 5: a) Selectivity of different target gases towards CS sensor, b) Response towards ammonia at various temperatures. c) Response and recovery plot of CS at 100 ppm of NH3, d) Change in resistance value of CS sensor on exposure to ammonia e) and f) Effect of concentration on response of CS sensor at different concentrations dynamic and static, respectively, g) Response reproducibility, and h) Stability measurements of CS sensor.

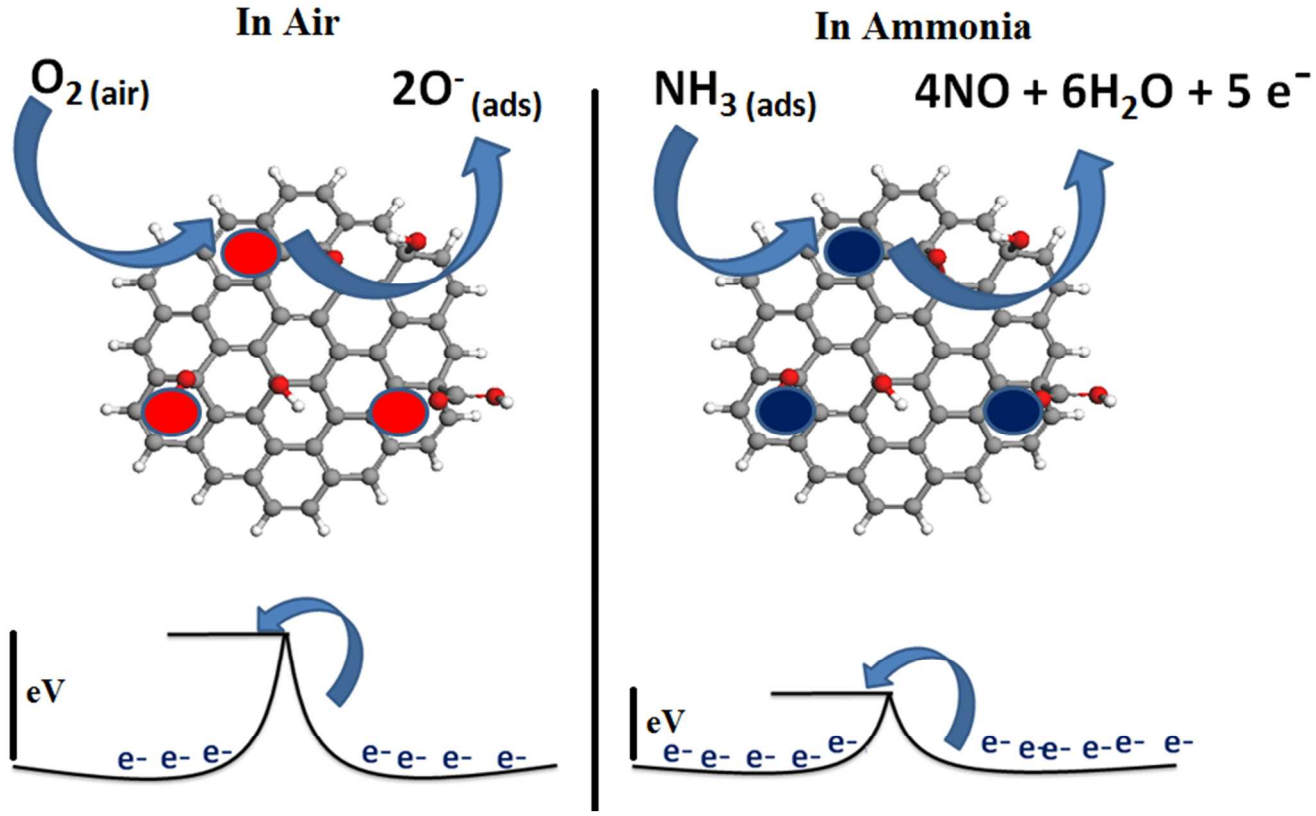

Figure 6: NH_3 sensing mechanism of CS sensor.

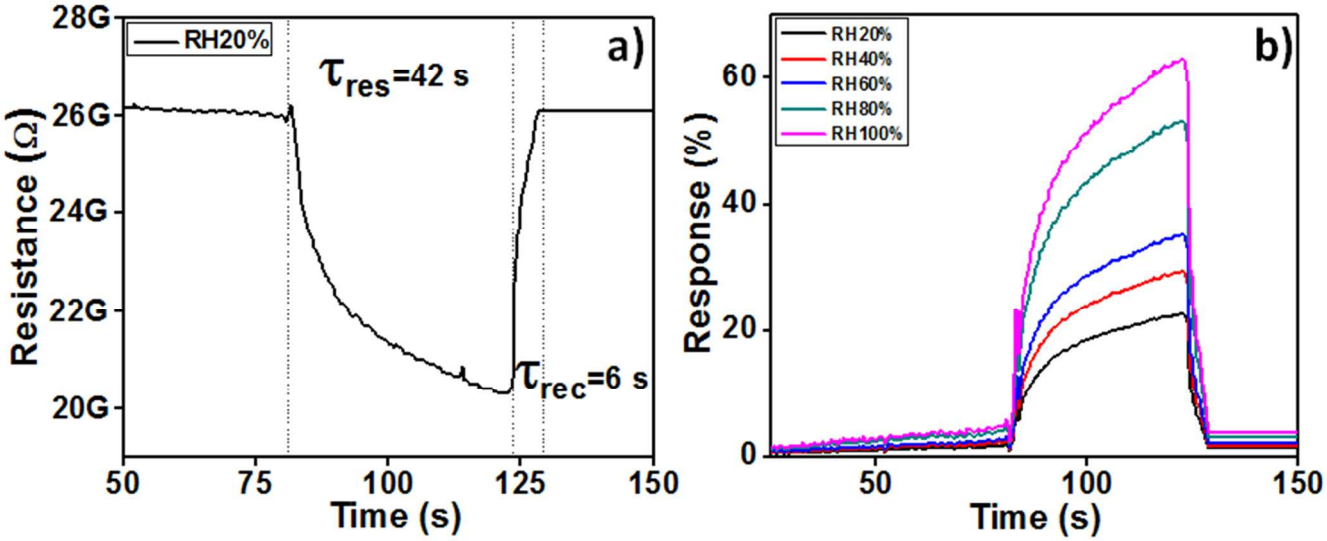

Fig. 7: Humidity sensing properties of CS sensor a) Variation of resistance of CS with respect to 20% RH, b) Response of the CS sensor with respect to various RH conditions.

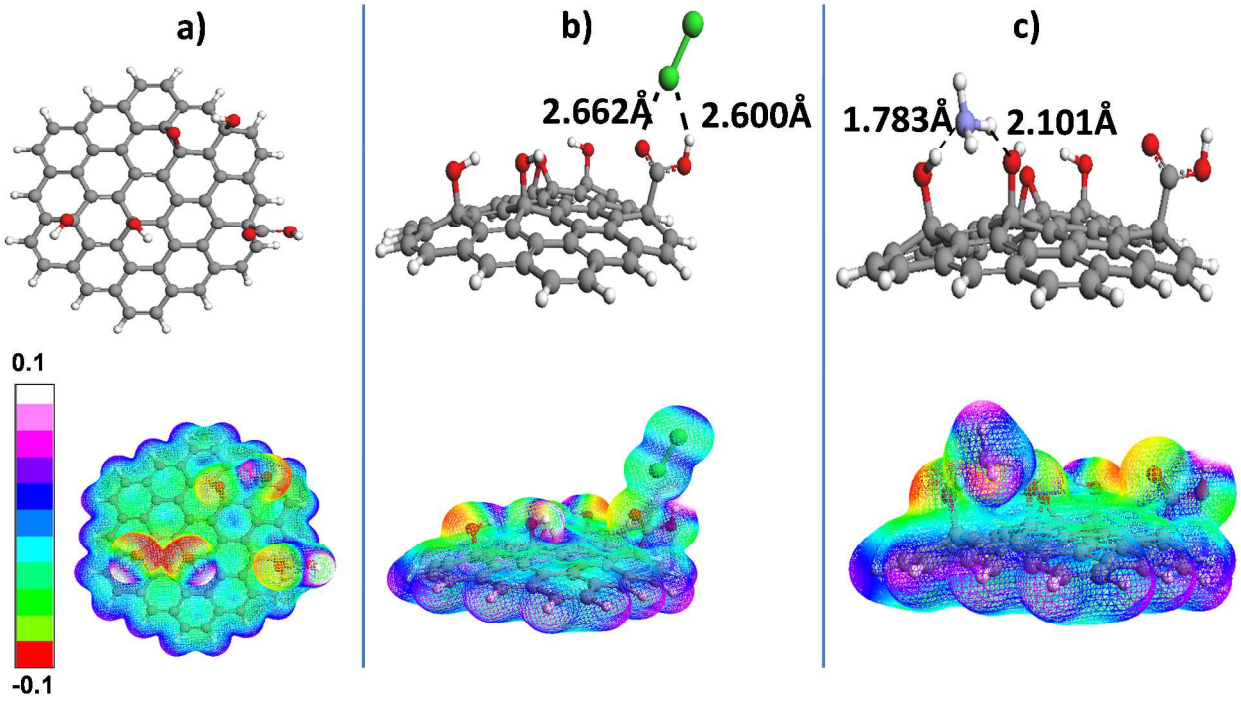

Figure 8: Optimized geometries and molecular electrostatic potentials (MEP) (isovalue = 0.005) of; a) CS, b) CS -Cl_2 and c) CS -NH_3. MEPs have been plotted using Arguslab 4.0.1 code.

TABLES:

Table 1: Comparison of responses of carbon, CNT's and graphene-based sensors found in the literature (RT-Room temperature i.e. ≈27°C).

Sensor Material	Concentration (ppm)	Response (%)	Temperature (°C)	Reference
Functionalised SWCNT	50	20.2	27	60
MWCNT–PEDOT:PSS	50	16	27	61
Graphene/Polyaniline	500	10	27	62
CNT	100	1.5	27	63
Graphene/polyaniline	100	10	27	64
BAX-CS1%	500	21	27	65
PANI:CNT	30	40	27	66
CS	100	50	80	This work

REFERENCES

1. Lelieveld J.; Evans J. S.; Fnais M.; Giannadaki, D. and Pozzer A. The contribution of outdoor air pollution sources to premature mortality on a global scale, *Nature*, **2015**, 525 (7569), 367-371.

2. Huang R. J.; Zhang, Y; Bozzetti, C.; Ho, K. F.; Cao, J. J.; Han, Y.; Daellenbach, K. R.; Slowik, J. G.; Platt, S. M.; Canonaco, F. and Zotter, P. High secondary aerosol contribution to particulate pollution during haze events in China, *Nature*, **2014**, 514 (7521), 218-222.

3. Rao, A. B. and Rubin, E. S. A technical, economic, and environmental assessment of amine-based CO_2 capture technology for power plant greenhouse gas control, *Env. Sci. tech.,* **2002**, 36 (20), 4467-4475.

4. Yang, G.; Lee, C.; Kim, J.; Ren, F. and Pearton, S. J. Flexible graphene-based chemical sensors on paper substrates, *Physical Chemistry Chemical Physics*, **2013**, 15 (60), 1798-1801.

5. Lu, G. and Hupp, J. T. Metal−Organic Frameworks as Sensors: A ZIF-8 Based Fabry−Pérot Device as a Selective Sensor for Chemical Vapors and Gases, *J. Americ. Chem. Soc.,* **2010**, 132 (23), 7832-7833.

6. Pejcic, B.; Eadington, P. and Ross, A. Environmental monitoring of hydrocarbons: a chemical sensor perspective, *Env. Sci. Tech.,* **2007**, 41 (18), 6333-6342.

7. Llobet, E. Gas sensors using carbon nanomaterials: A review, *Sens. Actuators B: Chem.,* **2013**, 179, 32-45.

8. Sun, Z. P.; Liu, L.; Li Z. and Jia, D. Z. Rapid synthesis of ZnO nano-rods by one-step, room-temperature, solid-state reaction and their gas-sensing properties, *Nanotech.,* **2006**, 17, 2266-2270.

9. Jadhav, V. V.; Patil, S. A.; Shinde, D. V.; Waghmare, S. D.; Zate, M. K.; Mane, R. S. and Han, S. H. Hematite nanostructures: Morphology-mediated liquefied petroleum gas sensors, *Sens. Actuators B: Chem.,* **2013**, 188, 669- 674.

10. Nakate, U. T.; Patil, P.; Bulakhe, R. N.; Lokhande, C. D.; Kale, S.N.; Naushad, Mu. and Mane, R. S. Sprayed zinc oxide films: Ultra-violet light-induced reversible surface wettability and platinum-sensitization-assisted improved liquefied petroleum gas response, *J. Colloid Interface Sci.,* **2016**, 480, 109-117.

11. Bhande, S. S.; Mane, R. S.; Ghule, A. V. and Han, S. H. A bismuth oxide nanoplate-based carbon dioxide gas sensor, *Scrip. Mater.,* **2011**, 65, 1081-1084

12. Rosmalini, A. K.; Li, Z.; Sadek, A. Z.; Rani, R. A.; Zoolfakar, A. S.; Field, M. R.; Ou, J. Z.; Chrimes, A. F. and Kalantar-zadeh, K. Electrospun Granular Hollow SnO_2 Nanofibers Hydrogen Gas Sensors Operating at Low Temperatures , *The J. Phys. Chem. C,* **2014**, 118, 3129-3139.

13. Yang, Y.; Liang, Y.; Wang, G.; Liu, L.; Yuan, C.; Yu, T.; Li, Q.; Zeng, F. and Gu, G. Enhanced Gas-Sensing Properties of the Hierarchical TiO_2 Hollow Microspheres with Exposed High-Energy {001} Crystal Facets, *ACS Appl. Mater. Interfaces,* **2015**, 7 (44), 24902-24908.

14. Dube, I.; Jime´nez, D.; Fedorov, G.; Boyd, A.; Chenko, I. G.; Paranjape, M. and Barbara, P. Understanding the electrical response and sensing mechanism of carbon-nanotube-based gas sensors, *Carbon*, **2015**, 87, 330-337.

15. Rigoni, F.; Drera, G.; Pagliara, S.; Goldoni, A. and Sangaletti, L. High sensitivity, moisture selective, ammonia gas sensors based on single-walled carbon nanotubes functionalized with indium tin oxide nanoparticles, *Carbon*, **2014**, 80, 356-363.

16. Slobodian, P.; Riha, P.; Lengalova, A.; Svoboda, P. and Saha, P. Multi-wall carbon nanotube networks as potential resistive gas sensors for organic vapor detection, *Carbon*, **2011**, 49, 2499-2507.

17. Cho, W. S.; Moon, S.; Paek, K. K.; Lee, Y. H.; Park, J. H. and Ju, B. K. Patterned multiwall carbon nanotube films as materials of NO_2 gas sensors, *Sens. Actuators B: Chem.,* **2006**, 119, 180-185.

18. Collins, P. G.; Bradley, K.; Ishigami, M. and Zettl, A. Extreme Oxygen Sensitivity of Electronic Properties of Carbon Nanotubes, *Science*, **2000**, 287, 1801-1804.

19. Yuan, Y.; Ding, Y.; Wang, C.; Xu, F.; Lin, Z.; Qin, Y.; Li, Y.; Yang, M.; He, X.; Peng, Q. and Li, Y. Multifunctional Stiff Carbon Foam Derived from Bread, *ACS Appl. Mater. Interfaces*, **2016**, 8(26), 16852-16861.

20. Rybarczyk, M.K.; Peng, H.J.; Tang, C.; Lieder, M.; Zhang, Q. and Titirici, M.M. Porous carbon derived from rice husks as sustainable bioresources: insights into the role of micro-/mesoporous hierarchy in hosting active species for lithium–sulphur batteries, *Green Chemistry*, **2016**, 18(19), 5169-5179.

21. Baughman, R. H.; Zakhidov, A. A. and De Heer, W. A. Carbon Nanotubes-the Route Toward Applications, *Science*, **2002**, 297 (5582), 787-792.

22. Neto, A. C.; Guinea, F.; Peres, N. M.; Novoselov, K. S. and Geim, A. K. The electronic properties of graphene, *Rev. Mod. Phy.,* **2009**, 81 (1), 109 (1-55).

23. Tangand, C. and Zhang, Q. Nanocarbon for Oxygen Reduction Electrocatalysis: Dopants, Edges, and Defects, *Adv, Mater.,* **2017**, 1604103 (1-9).

24. Xia, X.; Dongliang, C.; Yongqi, Z.; Jiye, Z.; Yu, Z.; Xiuli, W.; Yadong, W. Ze Xiang, S.; Jiangping, T. and Hong Jin, F. Generic Synthesis of Carbon Nanotube Branches on Metal Oxide

Arrays Exhibiting Stable High-Rate and Long-Cycle Sodium-Ion Storage, *Small*, **2016**, 12 (22), 3048-3058.

25. Shah, K. A. and Tali, B. A. Synthesis of carbon nanotubes by catalytic chemical vapour deposition: A review on carbon sources, catalysts and substrates, *Mater. Sci. Semi. Proc.,* **2016**, 41, 67-82.

26. Sun, D. L.; Hong, R. Y.; Wang, F.; Liu, J. Y. and Rajesh Kumar, M. Synthesis and modification of carbon nanomaterials *via* AC arc and dielectric barrier discharge plasma, *Chem. Eng. Journal*, **2016,** 283, 9-20.

27. Castro, H. P.; Souza, V. S.; Scholten, J. D.; Dias, J. H.; Fernandes, J. A.; Rodembusch, F. S.; dos Reis, R.; Dupont, J.; Teixeira, S. R. and Correia, R. R. Synthesis and Characterisation of Fluorescent Carbon Nanodots Produced in Ionic Liquids by Laser Ablation, *Chemistry–A European Journal,* **2016**, 22 (1), 138-143.

28. Mubarak, N. M.; Sahu, J. N.; Abdullah, E. C.; Jayakumar, N. S. and Ganesan, P. Microwave-assisted synthesis of multi-walled carbon nanotubes for enhanced removal of Zn (II) from waste water, *Res. on Chem. Inter.,* **2016**, 42 (4), 3257-3281.

29. Yang, Z. and Yu, Z. Hollow Carbon Nanoparticles of Tunable Size and Wall Thickness by Hydrothermal Treatment of α-Cyclodextrin Templated by F127 Block Copolymers, *Chem. Mater.,* **2013**, 25 (5), 704-710.

30. Choi, T.; Kim, S.; Lee, C. W.; Kim, H.; Choi, S.; Kim, S. H.; Kim, E.; Park, J. and Kim, H. Synthesis of carbon nanotube–nickel nanocomposites using atomic layer deposition for high-performance non-enzymatic glucose sensing, *Biosen. Bioelect.,* **2015**, 63, 325-330.

31. Nadagouda, M. N.; Speth, T. F. and Varma, R. S. Microwave-Assisted Green Synthesis of Silver Nanostructures, *Acc. Chem. Res.,* **2011**, 44 (7), 469-478.

32. Jiang, H.; Moon, K.; Zhang, Z.; Pothukuchi, S. and Wong, C. P. Variable Frequency Microwave Synthesis of Silver Nanoparticles, *J. Nano. Res.,* **2006,** 8 (1), 117-124.

33. Tsuji, M.; Hashimoto, M.; Nishizawa, Y.; Kubokawa, M. and Tsuji, T. Microwave-Assisted Synthesis of Metallic Nanostructures in Solution, *Chemistry–A European Journal,* **2005**, 11 (2), 440-452.

34. Nakate, U. T. and Kale, S. N. Microwave assisted synthesis and characterizations of $NiCo_2O_4$ nanoplates and Electrical, magnetic properties, *Materials Today: Proceedings*, **2016**, 3 (6), 1992-1998.

35. Timmer, B.; Olthuis, W. and Van Den Berg, A. Ammonia sensors and their applications—a review, *Sens. Actuators B: Chem.,* **2005**, 107 (2), 666-677.

36. Cui, S.; Pu, H.; Lu, G.; Wen, Z.; Mattson, E. C.; Hirschmugl, C.; Gajdardziska-Josifovska, M.; Weinert, M. and Chen, J. Fast and selective room-temperature ammonia sensors using silver nanocrystal-functionalized carbon nanotubes, *ACS Appl. Mater. Interfaces,* **2012**, 4 (9), 4898-4904.

37. Stankovich, S.; Dikin, D.A.; Piner, R.D.; Kohlhaas, K.A.; Kleinhammes, A.; Jia, Y.; Wu, Y.; Nguyen, S.T. and Ruoff, R.S., Synthesis of graphene-based nanosheets via chemical reduction of exfoliated graphite oxide, *Carbon*, **2007**, 45(7), 1558-1565.

38. Hyde, F. S. Graphene acid or Oxide, J. Soc. Chem. Ind., **1904**, 23, 300.

39. Johnson, J.A.; Benmore, C.J.; Stankovich, S. and Ruoff, R.S. A neutron diffraction study of nano-crystalline graphite oxide, *Carbon*, **2009**, 47(9), 2239.

40. Zhang, D.; Liu, A.; Chang, H. and Xia, B. Room-temperature high-performance acetone gas sensor based on hydrothermal synthesized SnO_2-reduced graphene oxide hybrid composite, *RSC Adv.*, **2015,** 5(4), 3016-3022.

41. Mutuma, B. K.; Rodrigues, R.; Ranganathan, K.; Matsoso, B.; Wamwangi, D.; Hümmelgen, I. A. and Coville, N. J. Hollow carbon spheres and a hollow carbon sphere/polyvinylpyrrolidone composite as ammonia sensors, *J. Mater. Chem. A*, **2017**, 5, 2539-2549.

42. Li, Y.; Hu, Y.; Li, H.; Chen, L. and Huang, X. A superior low-cost amorphous carbon anode made from pitch and lignin for sodium-ion batteries, *J. Mater. Chem. A,* **2016**, 4 (1), 96-104

43. Patidar, R.; Rebary, B. and Bhadu, G. R. Fluorescence characteristics of carbon nanoemitters derived from sucrose by green hydrothermal and microwave methods, *Spectrochimica Acta Part A: Mole. Biom. Spectro.,* **2016**, 169, 25-29.

44. Su, C.; Acik, M.; Takai, K.; Lu, J.; Hao, S. J.; Zheng, Y.; Wu, P.; Bao, Q.; Enoki, T.; Chabal, Y. J. and Loh, K. P. Probing the catalytic activity of porous graphene oxide and the origin of this behaviour, *Nat. Comm.,* **2012**, 3, 1298 (1-9).

45. Park, S.; An, J.; Jung, I.; Piner, R. D.; An, S. J.; Li, X.; Velamakanni, A. and Ruoff, R. S. Colloidal suspensions of highly reduced graphene oxide in a wide variety of organic solvents, *Nano letters*, **2009**, 9(4), 1593-1597.

46. Marcano, D. C.; Kosynkin, D. V.; Berlin, J. M.; Sinitskii, A.; Sun, Z.; Slesarev, A.; Alemany, L. B.; Lu, W. and Tour, J. M., Improved synthesis of graphene oxide, *ACS Nano*, **2010**, 4 (8), 4806-4814

47. Shen, J.; Long, Y.; Li, T.; Shi, M.; Li, N. and Ye, M. One-pot polyelectrolyte assisted hydrothermal synthesis of TiO_2-reduced graphene oxide nanocomposite, *Mater. Chem. and Physic.*, **2012**, 133(1), 480-486.

48. Navale, S. T.; Jadhav, V. V.; Tehare, K. K.; Sagar, R. U. R.; Biswas, C. S.; Galluzzi, M.; Liang, W.; Patil, V. B.; Mane, R. S. and Stadler, F. J. Solid-state synthesis strategy of ZnO nanoparticles for the rapid detection of hazardous Cl_2, *Sens. Actua. B: Chem.,* **2017**, 238, 1102–1110.

49. Navale, S. T.; Liu, C.; Gaikar, P. S.; Patil, V. B.; Sagar, R.U.R.; Du, B.; Mane, R. S. and Stadler, F. J. Solution-processed rapid synthesis strategy of Co_3O_4 for the sensitive and selective detection of H_2S, *Sens. Actua. B: Chem*, **2017**, 245, 524–532.

50. Zhang, D.; Jiang, C.; Li, P. and Sun, Y. E. Layer-by-Layer Self-assembly of Co_3O_4 Nanorod-Decorated MoS_2 Nanosheet-Based Nanocomposite toward High-Performance Ammonia Detection. *ACS Appl. Mater. Interfaces*, **2017**, *9* (7), 6462-6471.

51. Pawbake, A. S.; Waykar, R. G.; Late, D.J. and Jadkar, S. R. Highly transparent wafer-scale synthesis of crystalline WS_2 nanoparticle thin film for photodetector and humidity-sensing applications. *ACS Appl. Mater. Interfaces*, **2016**, 8(5), 3359-3365.

52. Zahab, A.; Spina, L.; Poncharal, P. and Marliere, C. Water-vapor effect on the electrical conductivity of a single-walled carbon nanotubes, *Mater. Phys. Rev. B*, **2000**, 62, 10000–10003.

53. Pati, R.; Zhang, Y.; Nayak , S. K. and Ajayan, P. M. Effect of H2O adsorption on electron transport in a carbon nanotubes, *Appl. Phy. Lett.,* **2002**, 81, 2638–2640.

54. Malard, L. M.; Pimenta, M. A.; Dresselhaus, G. and Dresselhaus, M. S. Raman spectroscopy in graphene, *Phys. Rep.,* **2009**, 473 51–87.

55. Chu, J.; Peng, X.; Feng, P.; Sheng, Y. and Zhang, J. Study of humidity sensors based on nanostructured carbon films produced by physical vapor deposition, *Sens. Actuators B: Chem.,* **2013**, 178 508– 513.

56. Afify, A. S.; Ahmad, S.; Khushnood, R. A.; Jagdale, P. and Tulliani, J. M. Elaboration and characterization of novel humidity sensor based on micro-carbonized bamboo particles, *Sens. Actuators B: Chem.,* **2017**, 239, 1251-1256

57. Vovusha, H.; Sanyal, S. and Sanyal, B. Interaction of Nucleobases and Aromatic Amino Acids with Graphene Oxide and Graphene Flakes, *The J. Phy. Chem. Lett.,* **2013**, 4, 3710-3718.

58. Vinayan, B. P.; Nagar, R. and Ramaprabhu, S. Synthesis and investigation of mechanism of platinum–graphene electrocatalysts by novel co-reduction techniques for proton exchange membrane fuel cell applications, *J. Mater. Chem.,* **2012**, 22, 25325-25334.

59. Frisch, M. J.; Trucks, G.W.; Schlegel, H.B.; Scuseria, G.E.; Robb, M.A.; Cheeseman, G. R.; Scalmani, G.; Barone, V.; Mennucci, B.; Petersson, G. A.; Nakatsuji, H.; Caricato, M.; Li, X.; Hratchian, H. P.; Izmaylov, A. F.; Bloino, J.; Zheng, G.; Sonnenberg, J. L.; Hada, M.; Ehara, M.; Toyota, K.; Fukuda, R.; Hasegawa, J.; Ishida, M.; Nakajima, T.; Honda, Y.; Kitao, O.; Nakai, H.; Vreven, T.; Montgomery, Jr., J. A.; Peralta, J. E.; Ogliaro, F.; Bearpark, M.; Heyd, J. J.; Brothers, E.; Kudin, K. N.; Staroverov, V. N.; Kobayashi, R.; Normand, J.; Raghavachari, K.; Rendell, A.; Burant, J. C.; Iyengar, S. S.; Tomasi, J.; Cossi, M.; Rega, N.; Millam, J. M.; Klene, M.; Knox, J. E.; Cross, J. B.; Bakken, V.; Adamo, C.; Jaramillo, J.; Gomperts, R.; Stratmann, R. E.; Yazyev, O.; Austin, A. J.; Cammi, R.; Pomelli, C.; Ochterski, J. W.; Martin, R. L.; Morokuma, K.; Zakrzewski, V. G.; Voth, G. A.; Salvador, P.; Dannenberg, J. J.; Dapprich S, Daniels, A.D.; Farkas, Ö; Foresman, J.B.; Ortiz, J.V.; Cioslowski, J.; Fox, D.J. *Gaussian 09*, Revision C.01 (Gaussian, Inc., Wallingford CT), (**2010**).

60. Dasari, B. S.; Taube, W. R.; Agarwal, P. B.; Rajput, M.; Kumar, A. and Akhtar, J. Room temperature single walled carbon nanotubes (SWCNT) chemiresistive ammonia gas sensor, *Sensors & Transducers*, **2015**, 190(7), 24-30.

61. Sharma, S.; Hussain, S.; Singh, S. and Islam, S. S. MWCNT-conducting polymer composite based ammonia gas sensors: A new approach for complete recovery process, *Sens. Actuators B: Chem.,* **2014**, 194, 213-219.

62. Tian, X.; Wang, Q.; Chen, X.; Yang, W.; Wu, Z.; Xu, X.; Jiang, M. and Zhou Z. Enhanced performance of core-shell structured polyaniline at helical carbon nanotube hybrids for ammonia gas sensor, *Appl. Phy. Lett.,* **2014**, 105, 203-109.

63. Nguyen, L. Q., Phan, P. Q.; Duong, H. N.; Nguyen C. D. and Nguyen, L. H. Enhancement of NH_3 Gas Sensitivity at Room Temperature by Carbon Nanotube-Based Sensor Coated with Co Nanoparticles, *Sensors,* **2013**, 13 (2), 1754-1762.

64. Wu, Z.; Chen, X.; Zhu, S.; Zhou, Z.; Yao, Y.; Quan, W. and Liu, B. Enhanced sensitivity of ammonia sensor using graphene/polyaniline nanocomposite, *Sens. Actuators B: Chem.,* **2013**, 178, 485-493.

65. Travlou, N.A. and Bandosz, T.J. Nanoporous carbon-composites as gas sensors: Importance of the specific adsorption forces for ammonia sensing mechanism, *Carbon,* **2017,** 121, 114-126.

66. Eising, M.; Cava, C.E.; Salvatierra, R.V.; Zarbin, A.J.G. and Roman, L.S. Doping effect on self-assembled films of polyaniline and carbon nanotube applied as ammonia gas sensor, *Sens. Actuators B: Chem.,* **2017**, 245, 25-33.

GRAPHICAL ABSTRAT: